

References and Notes

1. G. R. Hasle, C. B. Lange, *Diatom Res.* **7**, 37 (1992).
2. C. R. Tomas, *Identifying Marine Phytoplankton* (Academic Press, New York, 1997).
3. *C. granii*, *C. wailiesii*, and *C. radiatus* were collected from the North Sea (Germany) and cultivated as axenic unialgal cultures in an artificial seawater medium according to the recipe from the North East Pacific Culture Collection ([www.ocgy.ubc.ca/cccm//NEPCC/esaw.html](http://www.ocgy.ubc.ca/cccm//NEPCC/esaw.html)). *C. asteromphalus* was obtained from this culture collection.
4. R. W. Drum, H. S. Pankratz, *J. Ultrastruct. Res.* **10**, 217 (1964).
5. A. M. M. Schmid, B. E. Volcani, *J. Phycol.* **19**, 387 (1983).
6. J. Pickett-Heaps, A. M. M. Schmid, L. A. Edgar, in *Progress in Phycological Research*, F. E. Round, D. J. Chapman, Eds. (Biopress, Bristol, UK, 1990), vol. 7, pp. 1–169.
7. R. Gordon, R. W. Drum, *Int. Rev. Cytol.* **150**, 243 (1994).

8. N. Kröger, R. Deutzmann, M. Sumper, *Science* **286**, 1129 (1999).
9. N. Kröger, R. Deutzmann, C. Bergsdorf, M. Sumper, *Proc. Natl. Acad. Sci. U.S.A.* **97**, 14133 (2000).
10. N. Kröger, R. Deutzmann, M. Sumper, *J. Biol. Chem.* **276**, 26066 (2001).
11. A supplementary figure and details of experimental procedures are available on Science Online at [www.sciencemag.org/cgi/content/full/295/5564/2430/DC1](http://www.sciencemag.org/cgi/content/full/295/5564/2430/DC1).
12. C. T. Kresge, M. E. Leonowicz, W. J. Roth, J. C. Vartuli, J. S. Beck, *Nature* **359**, 710 (1992).
13. S. Mann, G. A. Ozin, *Nature* **382**, 313 (1996).
14. H. P. Lin, C. Y. Mou, *Science* **273**, 765 (1996).
15. H. Yang, N. Coobs, G. A. Ozin, *Nature* **386**, 692 (1997).
16. A. Monnier *et al.*, *Science* **261**, 1299 (1993).
17. G. Widawski, B. Rawiso, B. Francois, *Nature* **369**, 387 (1994).
18. S. Schacht, Q. Huo, I. G. Voigt-Martin, G. D. Stucky, F. Schüth, *Science* **273**, 768 (1996).
19. A. Imhof, D. J. Pine, *Nature* **389**, 948 (1997).

20. SEM images were obtained on a Leo 1530 field-emission scanning electron microscope. *Coscinodiscus* valves in statu nascendi were obtained from a growing cell culture by treating the harvested cells twice with hot 2% SDS–100 mM EDTA to remove intracellular material, membranes, and wall coatings. Cell walls were pelleted by low-speed centrifugation (1000g), washed repeatedly with water, and dried. Inspection for valves in different stages of morphogenesis was done by SEM screening.
21. H. Tanaka, *Phys. Rev. Lett.* **76**, 787 (1996).
22. G. Griffiths, *Fine Structure Immunochemistry* (Springer, New York, 1993).
23. J. D. Pickett-Heaps, D. H. Tippit, J. A. Andreozzi, *Biol. Cell.* **35**, 199 (1979).
24. I thank R. Fischer for technical assistance, E. Hochmuth and R. Deutzmann for mass spectrometry analysis, and W. Tanner for helpful discussions. This work was supported by the Deutsche Forschungsgemeinschaft (SFB 521-A2).

22 January 2002; accepted 21 February 2002

# Atomic-Level Observation of Disclination Dipoles in Mechanically Milled, Nanocrystalline Fe

M. Murayama,<sup>1\*</sup> J. M. Howe,<sup>1†</sup> H. Hidaka,<sup>2</sup> S. Takaki<sup>2</sup>

Plastic deformation of materials occurs by the motion of defects known as dislocations and disclinations. High-resolution transmission electron microscopy was used to directly reveal the individual dislocations that constitute partial disclination dipoles in nanocrystalline, body-centered cubic iron that had undergone severe plastic deformation by mechanical milling. The mechanisms by which the formation and migration of such partial disclination dipoles during deformation allow crystalline solids to fragment and rotate at the nanometer level are described. Such rearrangements are important basic phenomena that occur during material deformation, and hence, they may be critical in the formation of nanocrystalline metals by mechanical milling and other deformation processes.

Mechanical milling is a technique for producing metallic alloys with ultrafine grain sizes by severe plastic deformation (1–4). These nanocrystalline alloys have unique mechanical properties, such as hardnesses and yield strengths that are several times as large as those of conventional alloys, that make them attractive for a variety of applications (3–5). The mechanisms by which materials deform during mechanical milling to produce ultrafine grains are not known, although it is thought that turbulent shear processes requiring crystal rotation are operative and that disclinations contribute to this process (6, 7). Similarly, the reasons for the unusual mechanical properties are not fully understood,

but have been attributed to the nature of grain boundaries (5, 8–10), the fine grain size, and/or the presence of defects such as disclinations, dislocations, and twins (1–4, 7, 11–14). We report the use of high-resolution transmission electron microscopy (HRTEM) (15, 16) to directly observe the atomic structure of partial disclination dipoles in body-centered cubic (bcc) Fe that had undergone severe plastic deformation by mechanical milling.

Disclinations are special physical objects that serve as carriers of violation of rotational symmetry (6, 17). They are found throughout nature and are used to describe such diverse phenomena as the arrangement of molecules in liquid crystals (17, 18), the deformation behavior of metals (6, 7), polarization effects and diffraction of electromagnetic waves (19), displacements of Earth's crust (20), galactic structures (21), misorientation in heteroepitaxial diamond films (22), and so forth. Disclinations in crystalline materials can alternatively be described in terms of individual line defects in the atomic structure called

dislocations (23, 24). It is possible to image the atomic structures of defects such as dislocations in crystalline solids by means of HRTEM (15, 16). For example, HRTEM has been used to reveal the atomic structures of individual dislocations and arrays of dislocations such as grain boundaries in a variety of materials, including semiconductors and metal alloys, where their presence has a profound effect on the electro-optical and mechanical properties of the materials, respectively (15, 16). HRTEM has also been used to reveal the structure and behavior of disclinations in a variety of polymeric materials at the microscopic and molecular levels (18, 25). In contrast, the atomic structure of disclination defects in inorganic crystalline solids has rarely been directly observed (22, 26).

The procedure of making a mechanically milled, pure Fe powder has been described in detail (4). In summary, commercially pure Fe powder was mechanically milled with steel balls by using a planetary ball mill for 100 hours under an Ar gas atmosphere. During this process, the Fe powder is mashed between the steel balls and undergoes severe plastic deformation at high strain rates. After the fabrication process, the bcc Fe powder had a hardness of 850 on the Vickers scale. HRTEM specimens were prepared from the Fe powder by ion milling and were examined in a JEOL JEM-4000EX microscope equipped with a UHP40H pole-piece and operating at 400 kV. The point resolution of the microscope at Scherzer defocus (–49.0 nm) is 0.18 nm, and this is sufficient to image the atomic structure of bcc Fe when it is oriented such that the  $\kappa$  axis in the crystal structure is parallel to the viewing direction (Fig. 1).

Figure 2A shows a HRTEM image of the mechanically milled, nanocrystalline Fe powder. The image is ~20.5 nm wide. The grain that occupies most of the figure is in a  $\kappa$  orientation. The hexagonal arrangement of columns of Fe atoms in this orientation are visible as white spots, as in the simulated

<sup>1</sup>Department of Materials Science and Engineering, University of Virginia, Charlottesville, VA 22904–4745, USA. <sup>2</sup>Department of Materials Science and Engineering, Kyushu University, Fukuoka, 812-8581, Japan.

\*On leave from the National Institute for Materials Science, Tsukuba, 305-0047, Japan.

†To whom correspondence should be addressed. E-mail: jh9s@virginia.edu

image in Fig. 1B (27). White lines were drawn periodically along the three sets of edge-on  $\{110\}$  planes in the grain, and these are shown superimposed on the HRTEM image in Fig. 2B. Two sets of  $\{110\}$  planes running vertically in the figure are straight (or nearly so), but the set that is approximately horizontal in the figure bends considerably. Dark lines were drawn on all of the nearly horizontal, bent  $\{110\}$  planes in Fig. 2B to accurately indicate their positions. The black and white lines in Fig. 2B were removed from the HRTEM image and are shown separately in Fig. 2C for clarity. The discussion that follows emphasizes the bent  $\{110\}$  planes shown in Fig. 2C, but it should be remembered that these planes are derived from the actual atomic positions visible in Fig. 2A.

The arrows in Fig. 2C mark two wedge-shaped regions that together form a partial disclination dipole (6). The wedge-shaped regions are  $\sim 3.5$  nm apart. Each of the wedge-shaped regions contains a number of terminating  $\{110\}$  planes, which are individual dislocations with a Burgers vector  $b$ —the displacement vector that describes the magnitude and direction of their strain field (24)—of  $b = a/2\kappa$ . The partial dislocation dipoles in Fig. 2C appear to be wedge disclinations with a Frank vector  $w$ —the rotational vector that describes the distur-

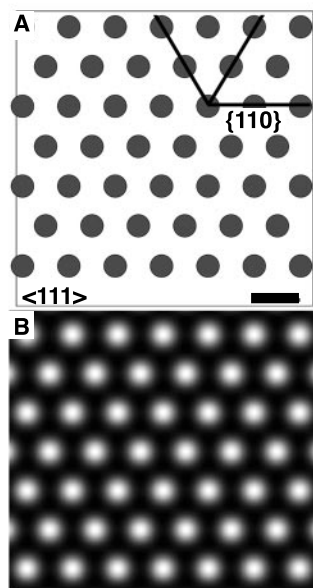


**Fig. 1.** (A) Projection of the atomic structure of bcc Fe oriented along a  $\kappa$  direction. The columns of Fe atoms spaced 0.248 nm apart form a hexagonal pattern and are clearly visible in this projection. Three sets of edge-on  $\{110\}$  planes of atoms are indicated by black lines. (B) Simulated HRTEM image of a 6.0-nm-thick crystal of bcc Fe oriented along the  $\kappa$  direction; microscope and specimen conditions were similar to those used to obtain the experimental image shown in Fig. 2A (27). Scale bar in (A), 0.248 nm.

tional power of the disclination—that is parallel to the defect line (in this case, the  $\kappa$  viewing direction). Unfortunately, it is not possible to exactly determine the wedge and twist components of the partial disclinations in Fig. 2 because a HRTEM image only reveals atomic displacement perpendicular to the electron beam direction and there may be displacements parallel to the beam that are not visible (15, 16). However, this image demonstrates that it is possible to directly observe the individual dislocations that constitute partial disclination dipoles in metals at the atomic level, even in mechanically milled powders that have undergone severe plastic deformation.

The set of terminating  $\{110\}$  planes that constitute the individual partial disclinations, such as the one circled and labeled I in Fig. 2C, can also be considered terminating tilt grain boundaries (24, 26). Compared with complete tilt grain boundaries, terminating tilt grain boundaries contain missing dislocations, and these are replaced by rotational

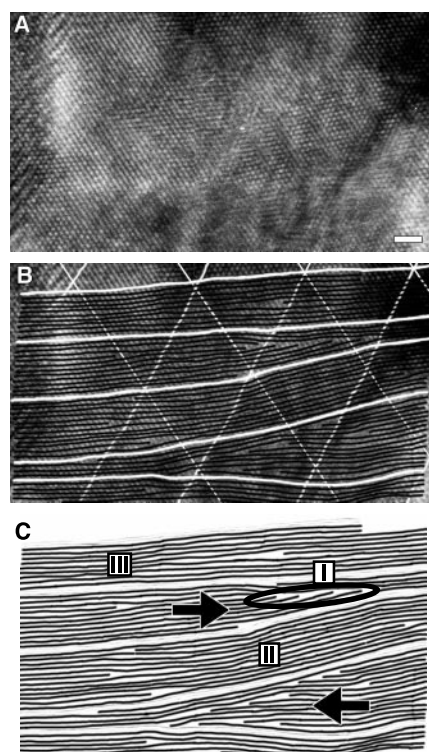


**Fig. 2.** (A) Experimental HRTEM image of mechanically milled, nanocrystalline Fe powder taken in a JEM-4000EX microscope near Scherzer defocus. The hexagonal arrangement of white spots in the image corresponds to columns of Fe atoms in a  $\kappa$  crystal orientation (see Fig. 1). (B) White lines shown superimposed periodically on the three sets of  $\{110\}$  planes in (A) to highlight the distortion of the nearly horizontal set of  $\{110\}$  planes. Black lines were also superimposed on this set of planes to clearly indicate their position. (C) The nearly horizontal black and white lines in (B) removed from the HRTEM image so that they are more clearly visible. The various labels are explained in the text. Scale bar in (A), 1.0 nm.

elastic deformation in the crystal (22). Such a configuration can be interpreted as a wedge of material added to or removed from an ideal crystal, as illustrated in Fig. 3, and this is evident from the wedge shape of the bent white lines in Fig. 2, B and C. The crystal rotation produced by the partial disclinations (or terminating tilt grain boundaries) in Fig. 2 is also evident. For example, the  $\{110\}$  planes located between the two partial disclinations (labeled II in Fig. 2C) are rotated  $\sim 9^\circ$  relative to the  $\{110\}$  planes located outside the dipole (such as the nearly horizontal planes labeled III in Fig. 2C). This observation provides direct confirmation that crystals can rotate and thereby undergo turbulent behavior during severe plastic deformation by the action of partial disclinations (6).

The terminating dark lines in Fig. 2C reveal the arrangement of individual dislocations that constitute the partial disclinations associated with the dipole in this figure, as well as other, isolated dislocations in the metal. It is not common to find terminating tilt grain boundaries in

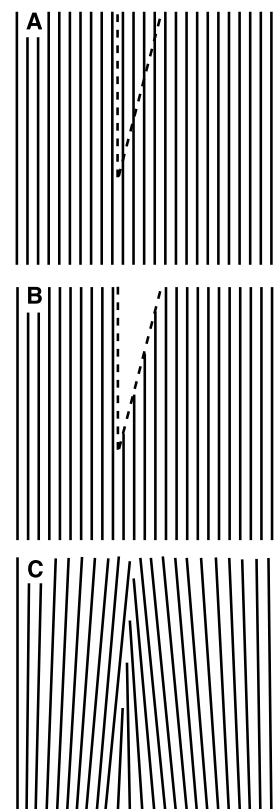


**Fig. 3.** Illustration of the elastic distortion associated with a partial wedge disclination (or terminating tilt grain boundary). (A) A set of planes in a perfect crystal, such as the perfect  $\{110\}$  planes seen in Fig. 1B. A wedge-shaped piece of material is removed from the crystal in (B), and the new surfaces are allowed to close in (C) to fill the wedge. The resulting crystal in (C) contains a terminating tilt grain boundary, i.e., a terminating array of edge dislocations, and considerable elastic distortion, which increases the elastic strain energy of the remaining solid.

materials, although a few cases have been reported in heteroepitaxial layers of semiconductors (22, 26). The presence of such defects in semiconductors was rationalized by comparing the energies of complete low-angle tilt grain boundaries with similar disclinations (22). It was shown that the disclinations are energetically more favorable when the misorientations between two crystals is only a few degrees, similar to the rotation in Fig. 2.

The introduction of partial wedge disclinations, dipoles, and other disclination defects into a metal during mechanical milling increases the stored elastic energy (6), as illustrated by the bent planes in Fig. 3. This stored elastic energy may be partly responsible for the unusually high enthalpy, which is on the order of one-third the heat of fusion, that is associated with mechanically milled Fe powder (2). Disclination defects can also contribute to the unusually high strength of fine-grained mechanically milled metals, because the large stress fields associated with them make it difficult for other deformation defects to move through the metal (23, 24). It is also likely that they contribute to the broadening of crystalline peaks in x-ray diffraction patterns commonly observed in mechanically milled metals (12, 14, 28).

The generation and interaction of partial wedge disclinations allows reorientation of crystal volumes only several nanometers in size. This mode of deformation on such a fine scale likely facilitates the fragmentation and reorientation process of metal grains undergoing severe plastic deformation (6, 29), leading to an ultrafine grain size. Thus, partial disclination defects such as those in Fig. 2 can contribute to both the deformation response and the strengthening of metals. The generation of partial disclination defects provides an alternative mechanism to grain boundary sliding, which has been suggested to allow rotation of nano-sized crystals during mechanical milling (30). It is not possible to determine exactly how the partial disclination dipoles in Fig. 2 formed from the HRTEM image, although the dislocations likely nucleated at preexisting defects such as grain boundaries or cell walls in the metal (29) and rearranged into the terminating arrays in Fig. 2.

Because HRTEM investigations have been performed on other mechanically milled powders, it is worth commenting why partial disclinations, such as those in Fig. 2, have not been previously reported. One reason for this may be that previous HRTEM investigations were performed on Cu and Cu-Fe alloys, where twinning is a common mode of deformation, and much attention was placed on the formation of twins, shear bands, and grain boundaries, rather than on disclination defects (13, 31). It may also be that the bcc crystal structure of Fe favors the formation of partial disclination defects over other possible types of defects in the material,

and that the high melting temperature of Fe limits movement and annihilation of the defects at ambient temperatures, thereby preserving them in the material for examination. These factors could be tested by performing HRTEM investigations of other high-melting temperature bcc metals and alloys.

We have used HRTEM to directly observe the atomic structure of partial disclination dipoles in bcc Fe that had undergone severe plastic deformation by mechanical milling and shown that the formation and migration of such partial disclinations during deformation allows crystalline solids to rotate and rearrange at the nanometer level. Such rearrangements are important basic phenomena that occur during material deformation, and hence may be critical in the formation of nanocrystalline metals by mechanical milling and other deformation processes. The formation of partial disclination dipoles and other disclination defects facilitates deformation under high stresses, and they also can cause considerable strengthening, owing to the interaction of their elastic stress fields with each other and with grain boundaries in the material. Thus, such disclination defects may make an important contribution to the unique material properties of nanocrystalline metal alloys produced by mechanical milling.

References and Notes

1. J. S. Benjamin, *Metall. Trans.* **1**, 2943 (1970).
2. H. J. Fecht, E. Hellstern, Z. Fu, W. L. Johnson, *Metall. Trans.* **A21**, 2333 (1990).
3. J. S. C. Jang, C. C. Koch, *Scripta Mater.* **24**, 1599 (1990).
4. Y. Kimura, H. Hidaka, S. Takaki, *Mater. Trans. Jpn. Inst. Met.* **40**, 1149 (1999).
5. H. Gleiter, *Prog. Mater. Sci.* **33**, 233 (1989).
6. A. E. Romanov, V. I. Vladimirov, in *Dislocations in Solids*, vol. 9, *Dislocations and Disclinations*, F. R. N. Nabarro, Ed. (North-Holland, Amsterdam, 1992), pp. 191–402.

7. A. A. Nazarov, A. E. Romanov, R. Z. Valiev, *Scripta Mater.* **34**, 729 (1996).
8. X. Zhu, R. Birringer, U. Herr, H. Gleiter, *Phys. Rev. B* **35**, 9085 (1987).
9. R. W. Siegel, G. J. Thomas, *Ultramicroscopy* **40**, 376 (1992).
10. E. A. Stern, *et al.*, *Phys. Rev. Lett.* **75**, 3874 (1995).
11. J. Schiotz, T. Rasmussen, K. W. Jacobsen, O. H. Nielsen, *Philos. Mag. Lett.* **74**, 339 (1996).
12. Y. H. Zhao, H. W. Sheng, K. Lu., *Acta Mater.* **49**, 365 (2001).
13. J. Y. Huang, Y. K. Wu, H. Q. Ye, *Acta Mater.* **44**, 1211 (1996).
14. A. Revesz, T. Ungar, A. Borbely, J. Lendvai, *Nanostruct. Mater.* **7**, 779 (1996).
15. P. R. Buseck, J. Cowley, L. Eyring, Eds., *High-Resolution Transmission Electron Microscopy and Associated Techniques* (Oxford Univ. Press, Oxford, 1988).
16. G. R. Anstis, J. L. Hutchison, in *Dislocations in Solids*, vol. 9, *Dislocations and Disclinations*, F. R. N. Nabarro, Ed. (North-Holland, Amsterdam, 1992), pp. 1–56.
17. M. Kléman, *Points, Lines and Walls* (Wiley, New York, 1983).
18. S. D. Hudson, *Curr. Opin. Colloid Interface Sci.* **3**, 125 (1998).
19. J. F. Nye, *Proc. R. Soc. A* **387**, 105 (1983).
20. T. W. Chou, H. J. Malasky, *Geophys. Res. B* **84**, 6083 (1979).
21. V. R. Parameswaran, *Specul. Sci. Technol.* **4**, 509 (1979).
22. J. Michler, Y. von Kaenel, J. Stiegler, E. Blank, *J. Appl. Phys.* **83**, 187 (1998).
23. M. J. Marcinkowski, *Philos. Mag.* **36**, 1499 (1977).
24. J. P. Hirth, J. Lothe, *Theory of Dislocations* (McGraw-Hill, New York, 1982).
25. P. M. Wilson, D. C. Martin, *Macromolecules* **29**, 842 (2000).
26. X. Jiang, C. L. Jia, *Appl. Phys. Lett.* **69**, 3902 (1996).
27. Supplementary figures and details of the HRTEM analyses are available on Science Online at [www.sciencemag.org/cgi/content/full/295/5564/2433/DC1](http://www.sciencemag.org/cgi/content/full/295/5564/2433/DC1).
28. K. Zhang, I. V. Alexandrov, R. Z. Valiev, K. Lu, *J. Appl. Phys.* **80**, 5617 (1996).
29. M. Seefeldt, *Rev. Adv. Mater. Sci.* **2**, 44 (2001).
30. J. Schiotz, F. D. Di Tolla, K. W. Jacobsen, *Nature* **391**, 561 (1998).
31. J. Y. Huang, *et al.*, *Acta Mater.* **45**, 113 (1997).
32. We acknowledge the helpful comments of J. P. Hirth and D. C. Martin on this work. Supported by the Ministry of Education, Culture, Sports, Science and Technology of Japan (M.M.) and by the National Science Foundation, Division of Materials Research (grant DMR-9908855) (J.M.H.).

25 October 2001; accepted 19 February 2002

# Orbital Influence on Earth's Magnetic Field: 100,000-Year Periodicity in Inclination

Toshitsugu Yamazaki<sup>1\*</sup> and Hirokuni Oda<sup>1</sup>

A continuous record of the inclination and intensity of Earth's magnetic field, during the past 2.25 million years, was obtained from a marine sediment core of 42 meters in length. This record reveals the presence of 100,000-year periodicity in inclination and intensity, which suggests that the magnetic field is modulated by orbital eccentricity. The correlation between inclination and intensity shifted from antiphase to in-phase, corresponding to a magnetic polarity change from reversed to normal. To explain the observation, we propose a model in which the strength of the geocentric axial dipole field varies with 100,000-year periodicity, whereas persistent nondipole components do not.

Long-term secular changes in Earth's magnetic field are important for understanding the energy sources of the geodynamo, which

produces the field. Although the geodynamo may be a self-sustained system within Earth's core that is maintained by heat and gravita-